Numerical Simulation of Vortex Flows Around Missile Configurations

P. Champigny, P. d'Espiney
ONERA, 29, avenue de la Division Leclerc
B.P. 72, 92322 Chatillon, Cedex, France

M. Brédif, H. Broussard
MATRA BAe Dynamics
37, avenue Louis Breguet
Boîte postale 1
78146 Velizy-Villacoublay Cedex
France

J.-P. Gillybœuf, Y. Kergaravat
EADS Aerospatiale Matra Missiles
Dept. E/SCG/N
2-18 rue Beranger
92320 Chatillon
France

SUMMARY

This paper describes the work achieved during the recent years to improve the quality of Navier-Stokes computations for industrial purpose. The main axes for improvement are the grid adaptation strategy, the turbulence modeling and the application to industrial missiles. A few years ago, Navier-Stokes computations were rarely run for external aerodynamics simulations. This is no longer true. Both industrial companies (EADS Aerospatiale Matra Missiles and MATRA BAe Dynamics France) now use it on a regular basis. Nevertheless some progresses are still necessary, especially for the prediction of the axial force.

1. INTRODUCTION

The accurate prediction of missile aerodynamic characteristics is a major task for the missile industry. It can rely on Euler computations only to a certain extent, depending on Mach number and angle of attack values. This approach has been widely used up to now. Nevertheless, Euler computations can not be used for all cases nor all characteristics. For example they are unable to accurately predict the axial force or the rolling moment coefficients. For this reason, a collaboration between ONERA and the French missile manufacturers EADS Aerospatiale Matra Missiles and MATRA BAe Dynamics France has been undertaken in order to assess Navier-Stokes simulations for missile external aerodynamics. In order to achieve this goal, the common study – hereafter called SIAM – has been divided into three parts.

The first part of the work is dedicated to grid adaptation in viscous regions. Two independent tools have been developed and validated. With the first tool, a multidomain mesh can be modified or refined in the boundary layers, remaining continuous between two domains. The second tool generates a new grid for each wake or vortex that has been detected in a flow. The new meshes overlap the initial one and the communication between all of them is achieved with the chimera technique.

In the second part of the work, the turbulence modeling has been handled with care. The number of turbulence models available in the literature is tremendous. Two categories have been retained (algebraic models and transport equation models) and one model has been selected for each category (Baldwin-Lomax and Spalart-Allmaras). An accurate and robust formulation of each model has been derived. Some examples related to generic configurations demonstrate the merits of these choices.

In the third part of the work, one turbulence model and one grid adaptation tool have been applied to industrial missiles.

The three components of the work have been separated only because it makes the presentation clearer but in fact they are closely combined. They are described in the next sections.

For all the configurations presented, the numerical solutions were obtained with the AEROLOG code developed by MATRA BAe Dynamics France [3] and with the FLU3M code developed at ONERA [1] in collaboration with EADS Aerospatiale Matra Missiles. The grids were built according to the general rules that have been found during the work to get grid independent solutions. The computations have been carried out with the wind tunnel conditions. The aerodynamic coefficients are always calculated in the missile reference frame.

The following notations are used:

CA	axial force coefficient (pressure and skin friction),
Cl	rolling moment coefficient,
CN	normal force coefficient,
Cp	pressure coefficient,
D	missile diameter,

Paper presented at the RTO AVT Symposium on "Advanced Flow Management: Part A – Vortex Flows and High Angle of Attack for Military Vehicles", held in Loen, Norway, 7-11 May 2001, and published in RTO-MP-069(I).

Report Documentation Page

Form Approved
OMB No. 0704-0188

1. REPORT DATE	2. REPORT TYPE	3. DATES COVERED
00 MAR 2003	**N/A**	**-**

4. TITLE AND SUBTITLE	5a. CONTRACT NUMBER
Numerical Simulation of Vortex Flows Around Missile Configurations	5b. GRANT NUMBER
	5c. PROGRAM ELEMENT NUMBER
6. AUTHOR(S)	5d. PROJECT NUMBER
	5e. TASK NUMBER
	5f. WORK UNIT NUMBER
7. PERFORMING ORGANIZATION NAME(S) AND ADDRESS(ES) **NATO Research and Technology OrganisationBP 25, 7 Rue Ancelle, F-92201 Neuilly-Sue-Seine Cedex, France**	8. PERFORMING ORGANIZATION REPORT NUMBER
9. SPONSORING/MONITORING AGENCY NAME(S) AND ADDRESS(ES)	10. SPONSOR/MONITOR'S ACRONYM(S)
	11. SPONSOR/MONITOR'S REPORT NUMBER(S)

12. DISTRIBUTION/AVAILABILITY STATEMENT
Approved for public release, distribution unlimited

13. SUPPLEMENTARY NOTES
Also see: ADM001490, Presented at RTO Applied Vehicle Technology Panel (AVT) Symposium held inLeon, Norway on 7-11 May 2001, The original document contains color images.

14. ABSTRACT

15. SUBJECT TERMS

16. SECURITY CLASSIFICATION OF:			17. LIMITATION OF ABSTRACT	18. NUMBER OF PAGES	19a. NAME OF RESPONSIBLE PERSON
a. REPORT	b. ABSTRACT	c. THIS PAGE			
unclassified	**unclassified**	**unclassified**	**UU**	**14**	

XCP/D position of the center of pressure from the nose,

α angle of attack,

β sideslip angle,

ϕ roll angle or circumferential angle.

2. MESH ADAPTATION

2.1. Introduction

Boundary layer separations, wakes and vortices are some of the viscous phenomena that occur around missiles. It is necessary to represent them accurately because they are of high importance for many missile aerodynamic characteristics. For example the axial force coefficient is linked to the boundary layer thickness; the aerodynamic characteristics of a lifting surface can be strongly affected if the surface is located within a wake or a vortex.

The accuracy of a numerical solution depends on the numerical scheme and the turbulence model, and also on the grid quality. The second point is considered here. Let us suppose that an initial multidomain conform mesh is available.

The boundary layers are defined through topological data (for example the wall boundary conditions) and physical data (for example the Reynolds number). The mesh is then modified or refined in the boundary layers with a tool named AMCOLI. AMCOLI does not require the initial flow in addition to the initial grid.

Grid adaptation in wakes and vortices is based on a different approach. The wakes and the vortices are partly described through topological and physical data and then they are detected in the initial flow with a tool named AMSITO. Moreover AMSITO does not modify the initial mesh but generates an overlapping grid for each wake and each vortex that has been detected. The new meshes and the initial one are not continuous and it is necessary to use the chimera technique in order to accomplish the communication between all of them.

The grid adaptation strategy is presented on figure 1.

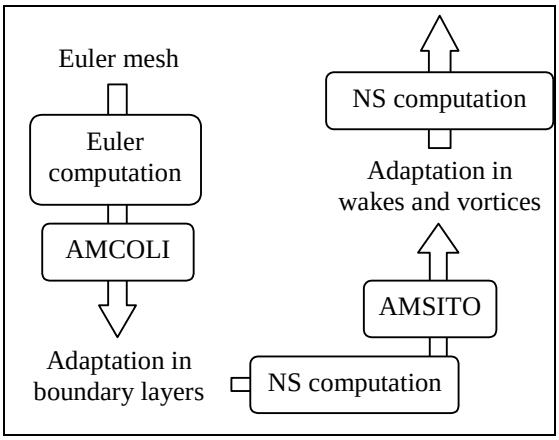

Figure 1 – Grid adaptation strategy

AMCOLI and AMSITO have been developed and validated with various configurations. They are completely independent of the CFD codes. In the next two paragraphs, their principle is exposed and some applications are presented.

2.2. Grid adaptation in boundary layers

The grid adaptation tool AMCOLI can be applied to transform an Euler mesh into a Navier-Stokes one, or to modify a Navier-Stokes grid according to new flow conditions. It also builds a flow in the boundary layers of the adapted mesh; outside the boundary layers, the initial flow is maintained if available otherwise the flow is uniform. AMCOLI gives some information to check the new mesh (smoothness, accuracy near the walls, …).

Compared to a classical grid generation tool, AMCOLI has the following advantages:

- the time required to create a Navier-Stokes mesh is much lower since the tool carries out many of the operations that are traditionally done by the user,
- the quality of the grid is improved by the use of the physical characteristics of the boundary layers,
- the construction of a flow in the adapted mesh should attenuate the convergence problems and accelerate the convergence itself.

AMCOLI requires the following data:

- the initial mesh (with or without the corresponding flow),
- some data which describe the gas and the flow (Prandtl number, Mach number, …),
- the grid points and grid lines which represent the beginning of the boundary layers,
- the description of the adaptation in the boundary layers (number of points, y^+ for the first cell, law for the distribution of points).

AMCOLI computes the main characteristics of the boundary layers (thickness, wall skin friction coefficient, …) with semi-empirical formulas. It works for very complicated topologies. It can handle axis singularities, C type and O type decompositions. The mesh adaptation applied in a domain is automatically extended to the adjacent domains, in all topological directions. The grid is modified only in the topological directions that are normal to a wall.

AMCOLI has been validated with various conventional and industrial configurations. Only one of them is presented as an illustration. An Euler mesh is built around a missile with a classical grid generation tool (figure 2). It contains 1 130 000 points. There are C-O type domains around the wings and the fins.

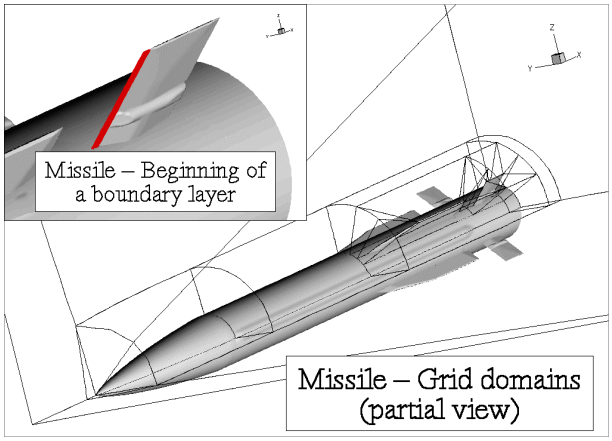

Figure 2 – Euler mesh around a missile

All the boundary layers are taken into account (over the fuselage, the four wings and the four fins). The Navier-Stokes mesh is obtained with AMCOLI after 17 minutes on one processor of a SGI Origin 2000. It contains 3 930 000 points and is smooth (figure 3).

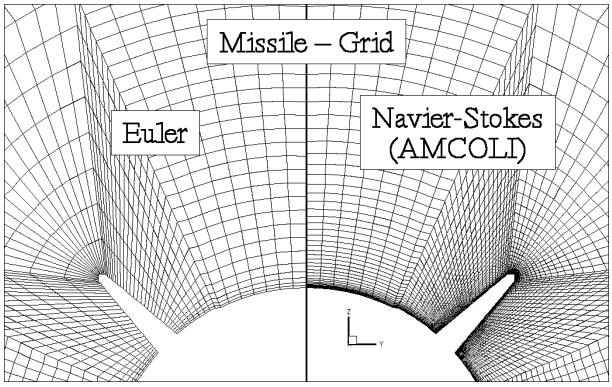

Figure 3 – Comparison between the initial Euler mesh and the Navier-Stokes mesh obtained with AMCOLI

After the validation of the tool, it was interesting to try to define some general rules which ensure that the numerical solution obtained on an adapted mesh does not depend on the grid adaptation parameters. For this reason, various parametric studies have been carried out on different configurations with the Baldwin-Lomax and the Spalart-Allmaras turbulence models (see §3). The conclusions, common to the different cases, can be summarized as follow:

- the law for the distribution of points (bigeometric or hyperbolic tangent) does not affect the solution,
- the boundary layers should contain at least 30 points,
- for the first cell, y^+ should be less than 3.

2.3. Grid adaptation in wakes and vortices

The grid adaptation tool AMSITO is able to detect wakes and vortices in a numerical flow and generates a new mesh for each of them. It also computes the flow in the new grids and gives some information to control what has been done.

AMSITO requires the following data:

- the initial mesh with the corresponding flow,
- the grid lines which represent the beginning of the wakes,
- some criteria to find the vortices and to follow the prescribed wakes,
- the description of the mesh adaptation (number of points, …).

From the grid line located at the trailing edge of a lifting surface, AMSITO builds a surface that represents the wake core (figures 4 and 5).

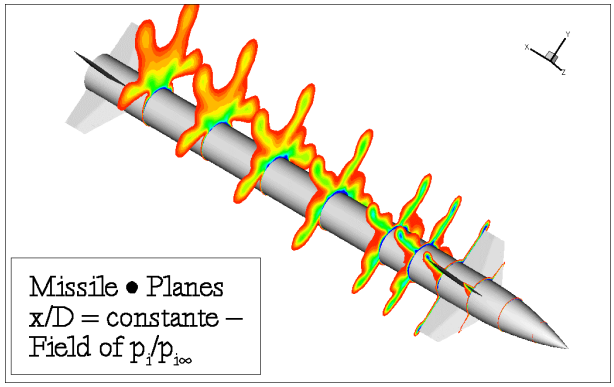

Figure 4 – Flow around a conventional missile

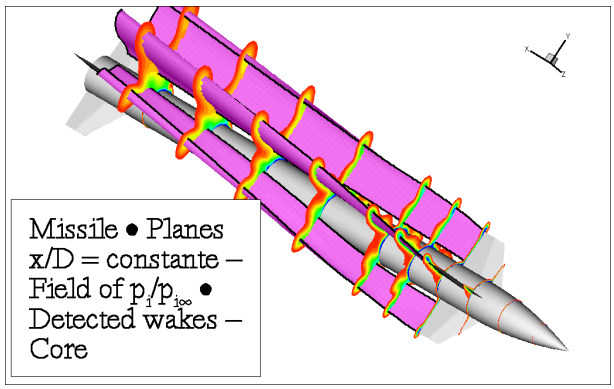

Figure 5 – Representation of the core of the wakes

This surface is then used to build two others, which represent the wake shape, and from which the overlapping mesh is created (figures 6 and 7).

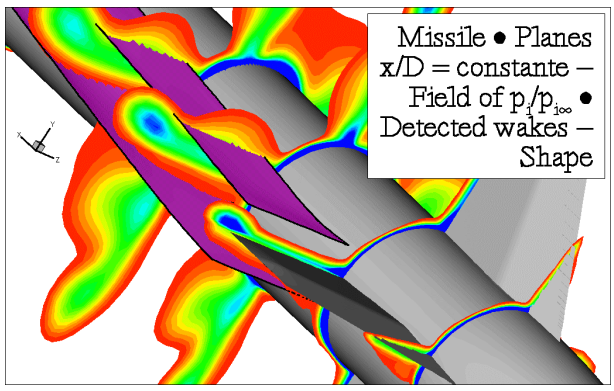

Figure 6 – Representation of the shape of a wake

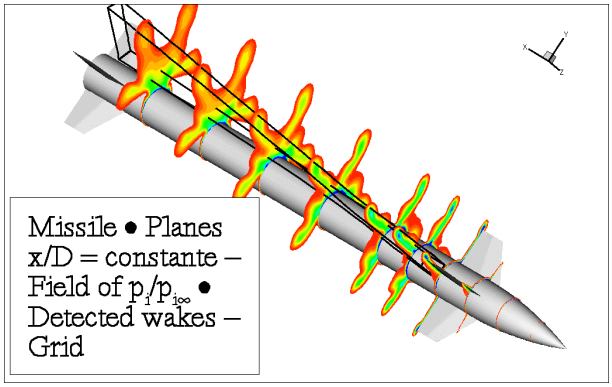

Figure 7 – Overlapping grid for a wake

The principle is similar for the vortices, except that their beginning is not prescribed by the user but automatically detected in the flow (figure 8).

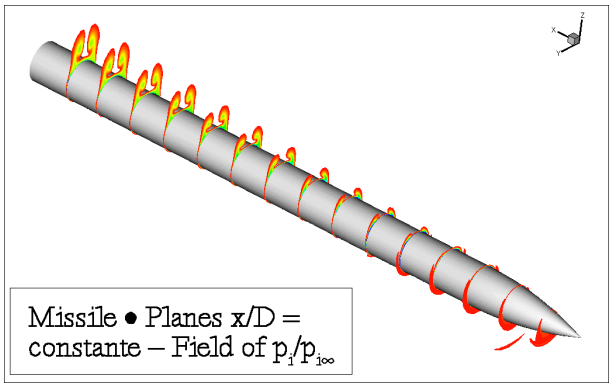

Figure 8 – Flow around a conventional missile

Then AMSITO generates for each vortex a line for the core, a surface that includes the vortex and finally the overlapping grid itself (figures 9 to 11).

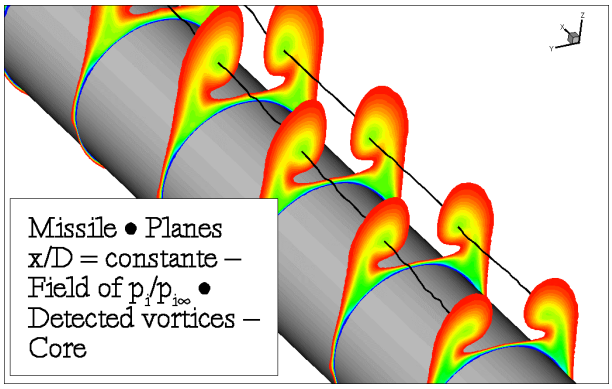

Figure 9 – Representation of the core of the vortices

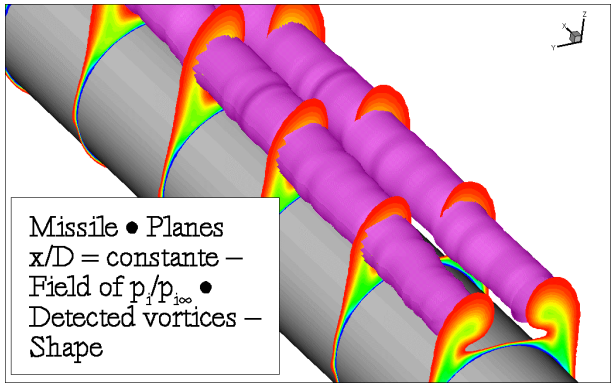

Figure 10 – Representation of the shape of the vortices

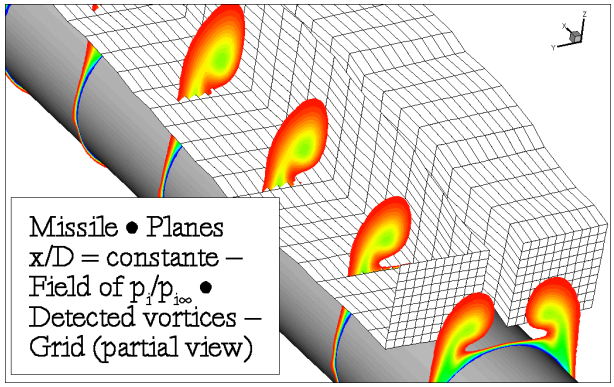

Figure 11 – Overlapping grids for the vortices

The detection of the physical structures in the flow (the core and the shape of the wakes and the vortices) is based on a combination of simple criteria (for example local minimum for the total pressure, local maximum for the rotational, absolute value of the helicity greater than 0.9, …). The criteria are defined by the user and the wakes and the vortices are automatically tracked.

The overlapping grids created by AMSITO do not match the original one. Thus it is necessary to use the chimera technique for the communication between all the meshes.

AMSITO has been validated with various configurations. Two examples concerning conventional missiles have been presented above. The initial meshes contain 2 075 700 points (wakes) and 2 552 500 points (vortices). The overlapping grids are obtained after 10 minutes on one processor of a SGI Origin 2000.

An additional analysis is in progress with the intention of finding some general conditions which guarantee that the numerical solution obtained on an adapted mesh is independent of the grid adaptation parameters. The following parameters are examined:

- the number of points in an overlapping grid in the streamwise direction of a wake or a vortex,
- the number of points in the two transversal directions,
- the size of an overlapping grid (is it necessary to overlap the whole wake or vortex ?),
- the size and the position of the region where the initial and the overlapping meshes communicate with each other.

2.4. Conclusion

Two grid adaptation tools have been developed and validated. They are independent of the CFD codes. The tool for the boundary layers is now widely used for industrial applications. The criteria for an accurate and mesh independent solution are known. The tool for wakes and vortices works but it is still investigated to find general and suitable utilization rules.

The accuracy of a numerical solution does not depend only on the grid quality. For this reason, the turbulence modeling must be handled with care.

3. TURBULENCE MODELING

As mentioned previously, two turbulence models have been mainly used for this study. They are the well-known Baldwin-Lomax model and the Spalart-Allmaras model (one transport equation). These models are considered as offering a good compromise between accuracy and computational cost for industrial applications.

3.1. Baldwin-Lomax model

This algebraic turbulence model represents a usual choice for external aerodynamics applications because of its minimal extra CPU cost and memory requirements. The estimate of the turbulent viscosity is based on a length scale, related to the maximum of the well-known Baldwin F function. In order to avoid an over-estimate of the turbulent viscosity when the flow separates (or in the vicinity of vortices), two modifications have been implemented: a cut-off distance for the search of the maximum of F and the well-known procedure of Degani and Schiff [2]. The model works even if there is more than one wall.

3.2. Spalart-Allmaras model

To overcome limitations of algebraic models, an eddy viscosity transport equation model has been implemented [4]. Baldwin and Barth recently rediscovered this class of one-equation models, proposed originally by Nee and Kovasznayin in the sixties. The Spalart-Allmaras model has been chosen due to the satisfactory results obtained over a wide range of flows and due to its numerical properties. In this model a step by step procedure is used to develop the transport equation for flows with increasing complexity. Moreover this one-equation model naturally takes history effects into account.

4. SIMULATION OF VORTEX FLOWS AROUND GENERIC CONFIGURATIONS

4.1. Ogive-cylinder configuration

The first test case consists of a very simple circular body (3D ogive + cylinder) at M = 2 and $\alpha = 10°$ [2] (figure 12). The missile length is 16 D. This configuration has been chosen because it represents a very simple vortical flow, which is convenient to compare different turbulence models. Moreover detailed experimental results and various computational results (Euler, laminar, k-ε) are available. Two grids, named g0 and g1, are used. The only difference is that the number of points on the circumference in grid g0 is half the number in grid g1. One Baldwin-Lomax + cut-off, two Baldwin-Lomax + Degani-Schiff and one Spalart-Allmaras computations have been performed.

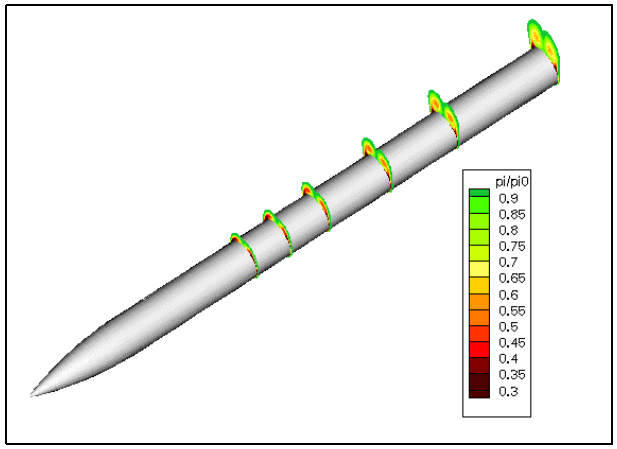

Figure 12 – Ogive-cylinder – Total pressure contours at M = 2, $\alpha = 10°$

Figure 13 shows that the vortical structure is globally correct. However the solutions obtained with the Baldwin-Lomax model can be very different (see the pressure distribution, figure 14), according to the variant used (Baldwin-Lomax + cut-off or Baldwin-Lomax + Degani-Schiff). Nevertheless the results are very close between Baldwin-Lomax + Degani-Schiff, Spalart-Allmaras and k-ε for the vortices, as well as for the local and global forces (figure 15). This last figure also shows the importance of taking the viscous effects (comparison with the Euler solution) and the turbulence (comparison with the laminar solution) into account.

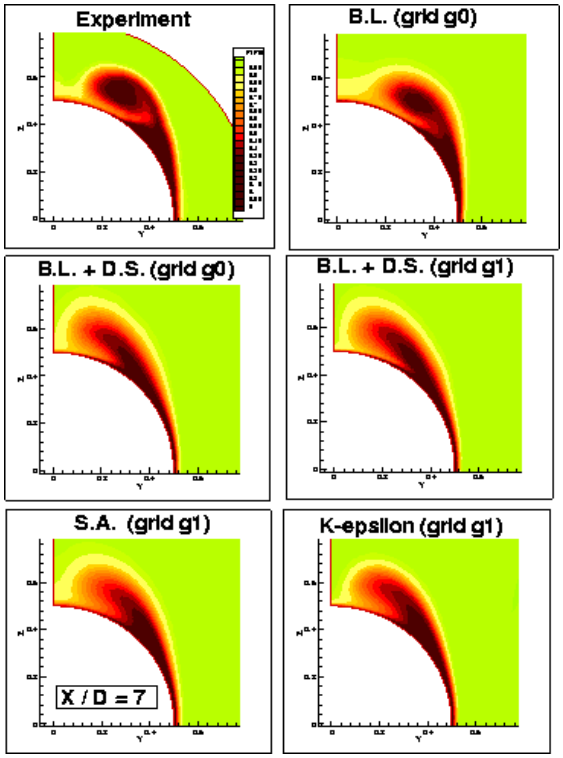

Figure 13 – Ogive-cylinder – Total pressure contours at M = 2, $\alpha = 10°$, X/D = 7

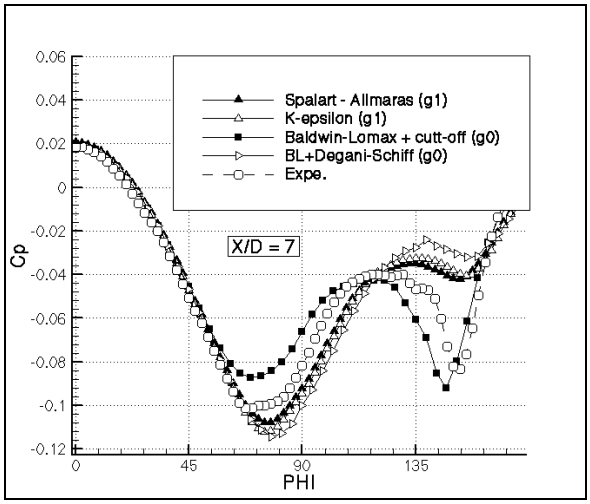

Figure 14 – Ogive-cylinder – Pressure distribution at M = 2, α = 10°, X/D = 7

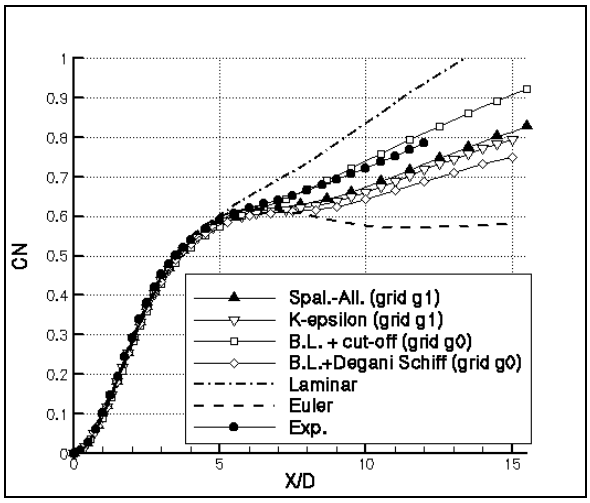

Figure 15 – Ogive-cylinder – Normal force coefficient at M = 2, α = 10°

4.2. Body-fin configuration

The second test case is a body-fin missile at M = 2 and ϕ = 22.5° (non-symmetric roll angle). The forebody vortices act on the fins (figure 16). They can modify the aerodynamic characteristics of the missile. In particular they create an induced rolling moment. For this reason it is interesting to study this configuration. Euler and Spalart-Allmaras computations have been carried out with the same grid, which contains around 1 000 000 points. The missile length is 16 D.

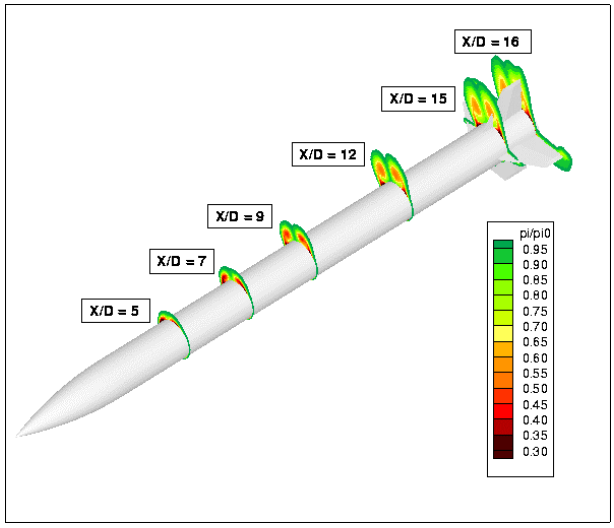

Figure 16 – Body-fin – Spalart-Allmaras solution at M = 2, α = 11.4°, ϕ = 22.5°

The prediction of the normal force (figure 17) and the position of the center of pressure (figure 18) is very good for the Spalart-Allmaras computations, and surprisingly not so bad for the Euler ones. This can be explained by the fact that in the Euler solutions the body normal force is underestimated (see §4.1), whereas the fins normal force is overestimated (no or smaller effect of the vortices).

The situation is not the same for the rolling moment (figure 19). The discrepancies with the experimental results are very small for the Spalart-Allmaras results and much higher for the Euler results. This shows that the accurate prediction of the rolling moment requires the modeling of the viscous effects. It is not surprising since the rolling moment is highly dependent on the individual contribution of each fin.

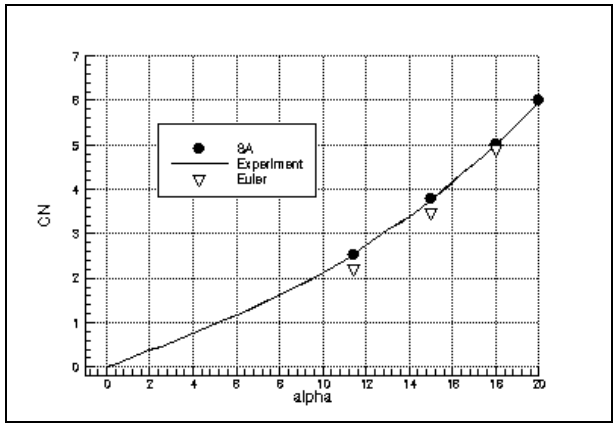

Figure 17 – Body-fin – Normal force coefficient at M = 2, ϕ = 22.5°

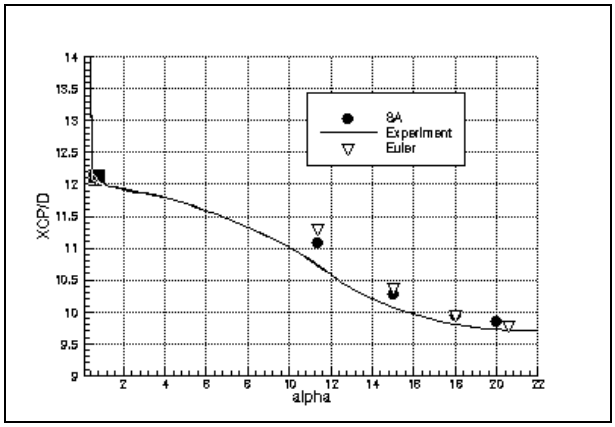

Figure 18 – Body-fin – Position of the center of pressure at M = 2, ϕ = 22.5°

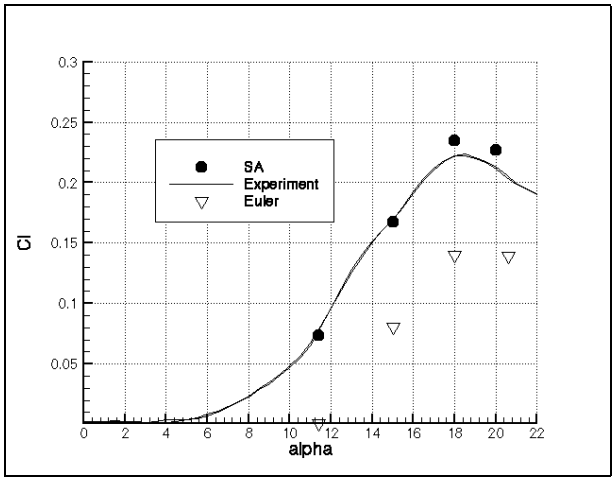

Figure 19 – Body-fin – Rolling moment coefficient at M = 2, ϕ = 22.5°

It is interesting to continue the analysis with the axial force coefficient. The difference between the Spalart-Allmaras and the experimental results is about 6%. As an indication, the discrepancy is almost zero for M = 3 and M = 4.5.

CA	M = 2 α = 0°	M = 3 α = 0°	M = 4.5 α = 0°
Experiment	0.307	0.263	0.23
Spalart-Allmaras model	0.32 (+6%)	0.265 (< 1%)	0.231 (< 1%)

4.3. Canard-body-fin configuration

The last test case is a canard-body-fin missile at M = 2 and ϕ = 45°. It represents a more realistic configuration since different kinds of vortices act on the fins (figure 20). Euler and Baldwin-Lomax + cut-off computations have been run with the same grid, which contains around 4 million points. The missile length is 16 D.

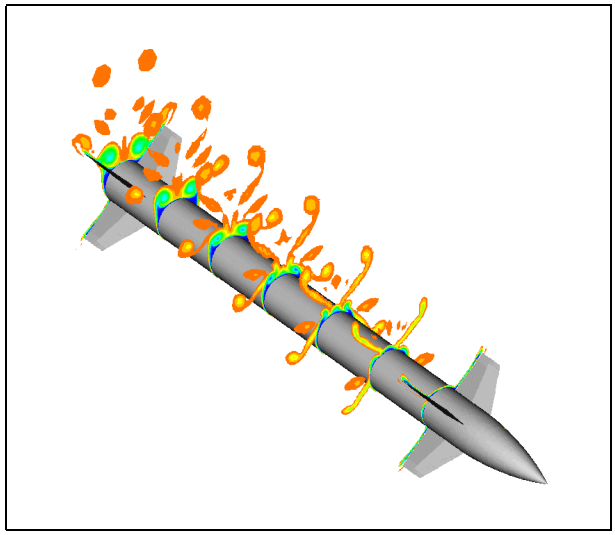

Figure 20 – Canard-body-fin configuration –Total pressure contours at M = 2, α = 10°, ϕ = 45°

Figure 21 shows the complex vortical structure, for a section between the canards and the tail fins. Again, only a Navier-Stokes (Baldwin-Lomax) solution can give a detailed and representative description of this vortical structure. Nevertheless, in the Euler solution some vortices are present, those coming from the wake of the forward canards.

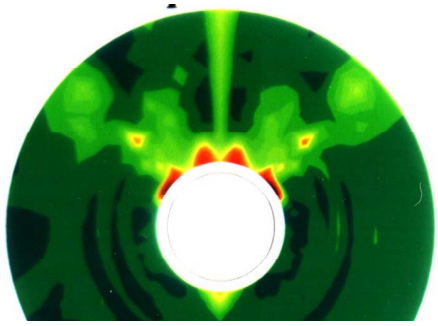

a – Experiment

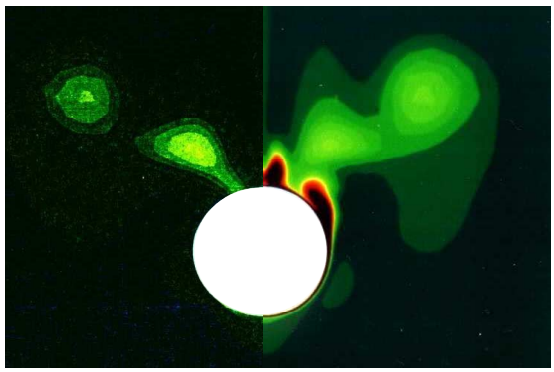

b – Euler (left) and Navier-Stokes (right) solutions

Figure 21 – Canard-body-fin – Total pressure contours at M = 2, α = 10°, ϕ = 45°, X/D = 10

The normal force coefficient and the position of the center of pressure are well predicted by both the Euler and the Navier-Stokes computations (figures 22 and 23). Is it the same for the loads on the fins ? In fact these loads are strongly affected by the vortices acting on the fins. For this reason the Euler computations should give bad quality results, which is

confirmed on figure 24. On the contrary, the Baldwin-Lomax results are very accurate.

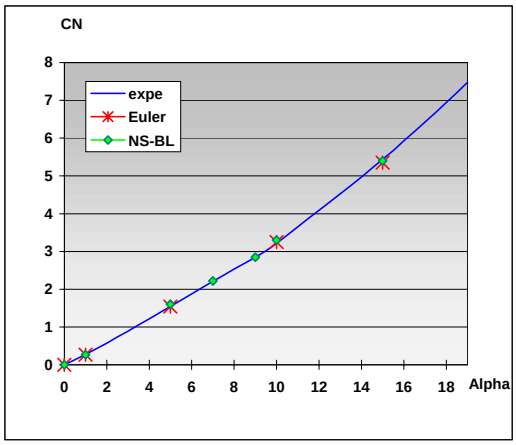

Figure 22 – Canard-body-fin – Normal force coefficient at M = 2, ϕ = 45°

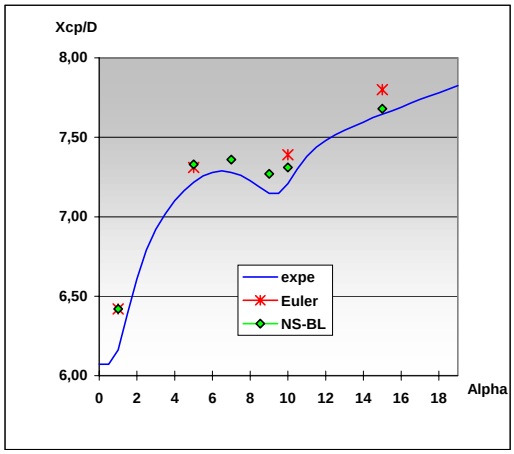

Figure 23 – Canard-body-fin – Position of the center of pressure at M = 2, ϕ = 45°

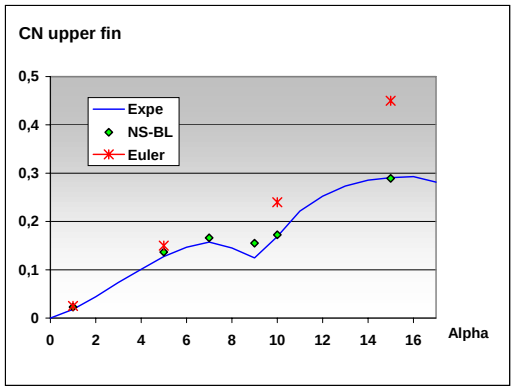

Figure 24 – Canard-body-fin – Fin normal force at M = 2, ϕ = 45°

4.4. Conclusions

Generic configurations have been studied for supersonic flows and various angles of attack.

For the ogive-cylinder configuration, a detailed study has been performed at α = 10°. The normal force coefficient induced by the vortical flow which develops on the leeward side is very sensitive to the viscous effects and to the turbulence model. None of the models is completely satisfactory: the Baldwin-Lomax model needs specific handling of the cut-off parameter whereas the Spalart-Allmaras and k-ε (Jones-Launder) models lead to results that are very close one to the other but overestimate the turbulent viscosity.

Taking the vortical flow into account is also important to predict the rolling moment on configurations with rear fins. For both the Baldwin-Lomax and the Spalart-Allmaras models a good estimate of this coefficient has been obtained. However the vortical flow has no visible effect on global longitudinal characteristics (CN and XCP/D). This is shown by the good prediction obtained with Euler calculations.

5. SIMULATION OF COMPLEX FLOWS AROUND INDUSTRIAL CONFIGURATIONS

The aim is to evaluate the improvement in the prediction and the quality of the results on configurations which are representative of two main families of missiles:

- the cruciform supersonic missiles,
- the stealth subsonic cruise missiles.

It has been interesting to assess the generality, the robustness and user-friendliness of the new developed tools. All the Navier-Stokes computations have been carried out with the Baldwin-Lomax + cut-off model.

5.1. Cruciform Supersonic Missile

The configuration is displayed on figure 25.

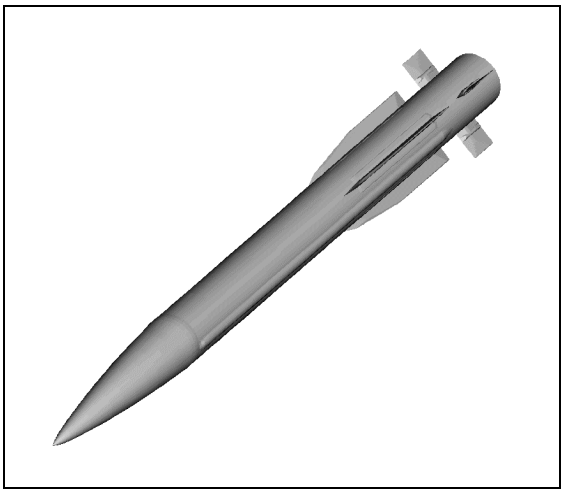

Figure 25 – Cruciform supersonic missile

Various computations have been run with both the FLU3M and the AEROLOG codes at M = 3.02, ϕ = 22.5° for different angles of attack. The mesh used is a 4 million point mesh in which the whole boundary layer developments are taken into account (above the fuselage, the wings and the fins). Starting with an Euler mesh, it has been generated thanks to AMCOLI in 1.5 hours on one processor of a SGI Origin 2000. The

computational time needed to get the result for one angle of attack is about 180 hours on the same machine.

Global aerodynamic loads depending on the angle of attack are displayed on figure 26 for the normal force coefficient, on figure 27 for the rolling moment, and on figure 28 for the position of the center of pressure. The numerical results are in good agreement with the experimental data. The maximal discrepancy on the prediction of the normal force coefficient is about 3%. For the prediction of the position of the center of pressure, the accuracy is about 0.1 D.

The prediction of the rolling moment coefficient, though less accurate than for the normal force coefficient, is correct. The global curve shape is well predicted. Values are in fair agreement with experiments, except for the angles of attack around 10°.

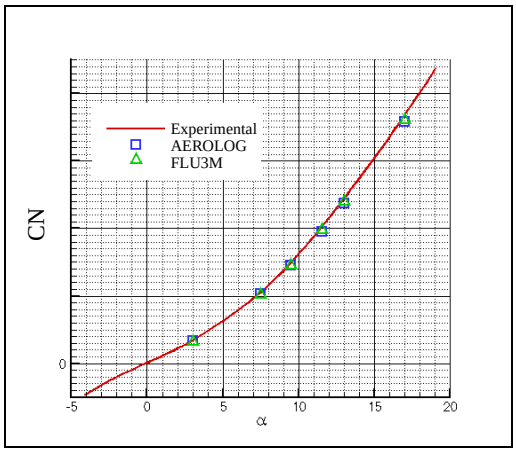

Figure 26 – Cruciform supersonic missile – Normal force coefficient at M = 3.02, ϕ = 22.5°

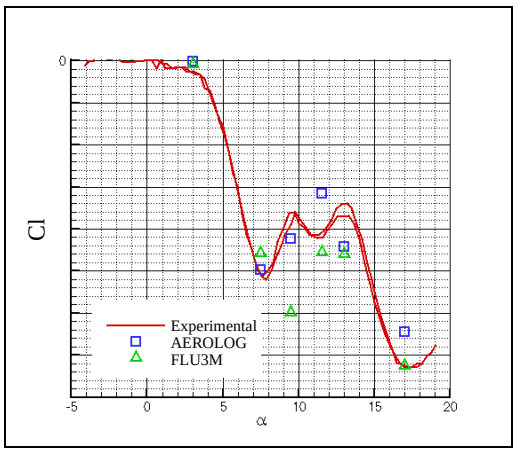

Figure 27 – Cruciform supersonic missile – Rolling moment coefficient at M = 3.02, ϕ = 22.5°

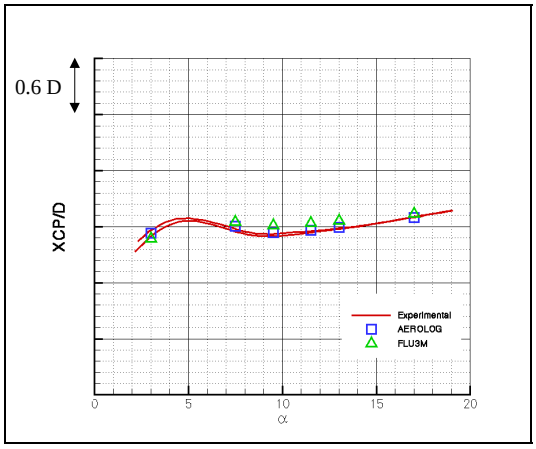

Figure 28 – Cruciform supersonic missile – Position of the center of pressure at M = 3.02, ϕ = 22.5°

The discrepancies in results obtained before this study are displayed in terms of rolling moment coefficient in the array below. One can see the improvement of the prediction of the rolling moment coefficient: the Euler computations were leading to an average discrepancy of 94%, whereas the Navier-Stokes results were accurate at an average rate of 39%. Considering the new results, the difference between the experimental data and the numerical results is included between 0 and 24%. This improvement in the prediction of the rolling moment coefficient may be due to the use of a different mesh (finer O type mesh created according to the general rules obtained in §2.2, each lifting surface being considered as viscous), to the modification of the Baldwin-Lomax model formulation, and also to the use of a different numerical scheme.

	Discrepancy of the prediction
Euler computations	94%
Navier-Stokes computations (before this study – SIAM)	39%
Navier-Stokes computations (after this study – SIAM)	0 to 24%

One problem remains concerning the prediction of the axial force coefficient. As one can see on figure 29 representing the axial force coefficient prediction for different angles of attack, the prediction is less than 10% accurate, which is not enough for industrial purpose.

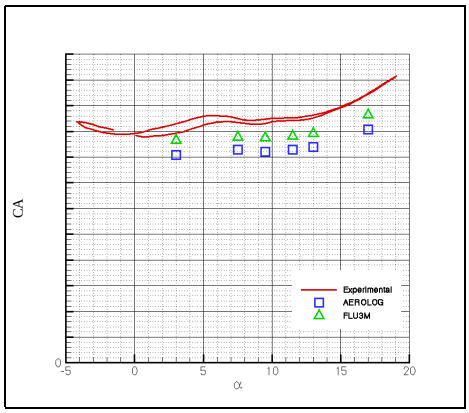

Figure 29 – Cruciform supersonic missile – Axial force coefficient at M = 3.02, ϕ = 22.5°

On the figures 30 and 31, the total pressure field is represented in two sections of the flow at $\alpha = 9.5°$ (X/D = 11.6 located around the wings and X/D = 14.5 located at the rear part of the missile). On figure 30, two different phenomena can be seen: there is an interaction between the forebody vortices and the wings on the upper side of the missile. Side vortices are also developing. The rolling angle of the flow acts on the development of these vortices. On the lower-right wing, the vortex is spreading since the fuselage hides it. On the lower-left wing, the vortex is thrown onto the fuselage, and thus it is not spread at all. On the figure 31, the forebody vortices, the side vortices of the wings and the wakes of the wings have interacted with the fins. The side vortices of the fins and their wakes can be seen. The vortex located at the upper-right side of the missile is less powerful than the one located at the upper-left side. This is due to the fact that the forebody vortex on the left side and the side vortices on the upper-left wing and fin are rotating in the same direction whereas on the upper-right side the vortices are counter-rotating.

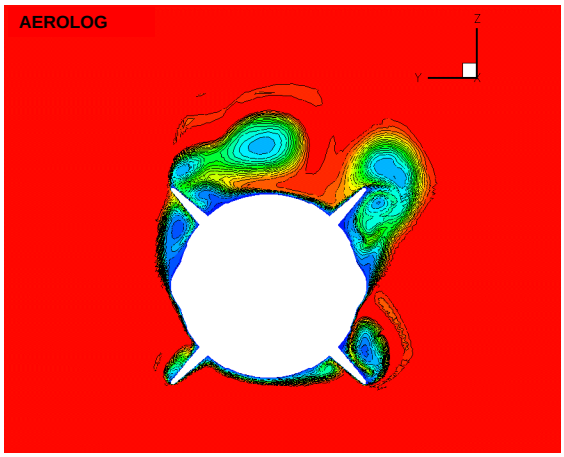

Figure 30 – Cruciform supersonic missile – Total pressure contours at M = 3.02, $\alpha = 9.5°$, $\phi = 22.5°$, X/D = 11.6

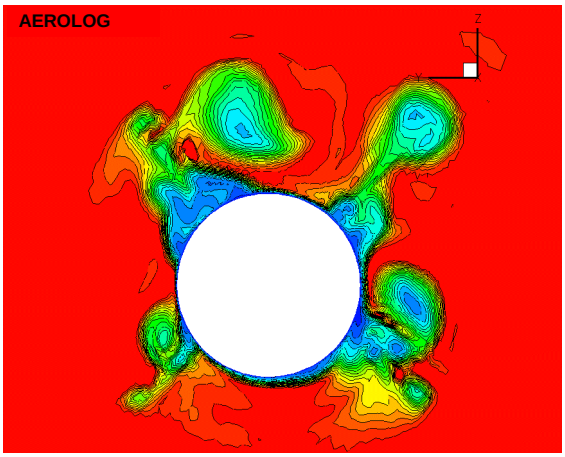

Figure 31 – Cruciform supersonic missile – Total pressure contours at M = 3.02, $\alpha = 9.5°$, $\phi = 22.5°$, X/D = 14.5

Some other computations have been run with FLU3M. They correspond to a specified angle of attack ($\alpha = 15°$) and different roll angles for M = 3.02. Global aerodynamic loads are displayed on figures 32 to 34. The normal force coefficient, the rolling moment coefficient and the position of the center of pressure are successively displayed.

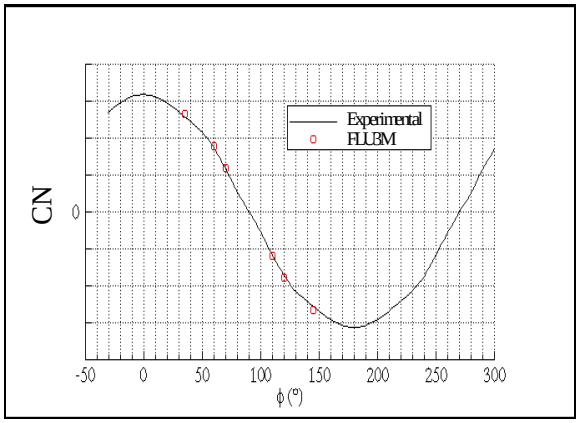

Figure 32 – Cruciform supersonic missile – Normal force coefficient at M = 3.02, $\alpha = 15°$

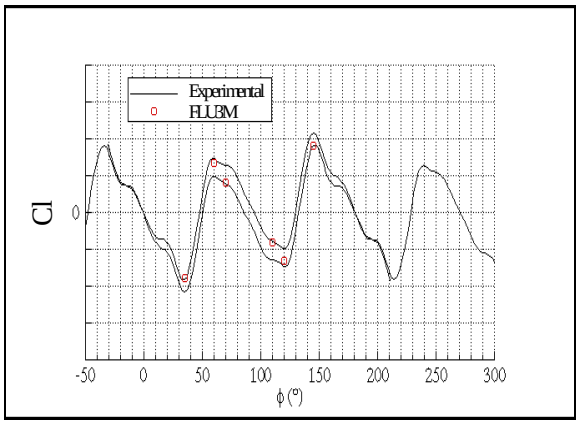

Figure 33 – Cruciform supersonic missile – Rolling moment coefficient at M = 3.02, $\alpha = 15°$

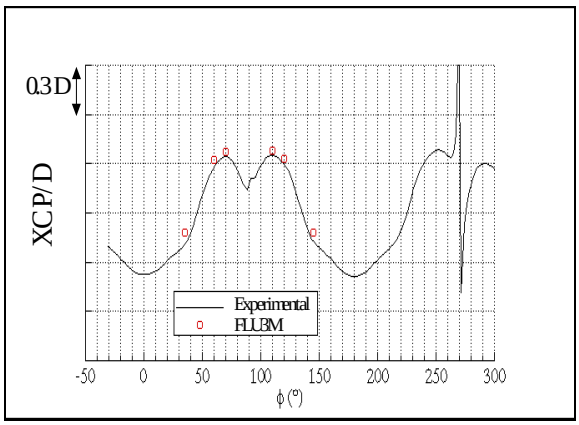

Figure 34 – Cruciform supersonic missile – Position of the center of pressure at M = 3.02, $\alpha = 15°$

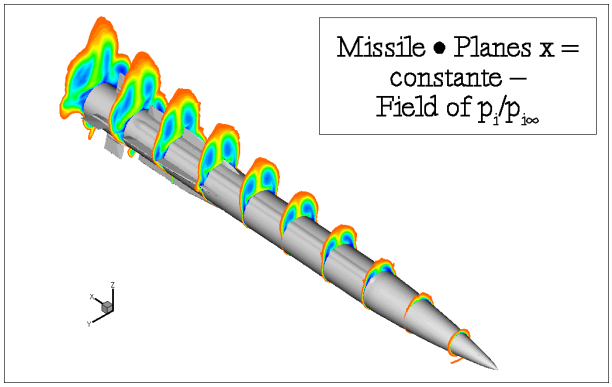

Figure 35 – Cruciform supersonic missile – Total pressure contours at M = 3.02, $\alpha = 15°$, $\phi = 60°$

The numerical results are in a good agreement with the experimental data. On the figure 35, the total pressure is displayed at $\phi = 60°$. This allows to well understand the complexity of the flow through the interaction of the vortices (forebody, side edge) and the wakes with the wings and the fins.

5.2. The Stealth Subsonic Cruise Missile

The configuration looks like the one displayed on figure 36.

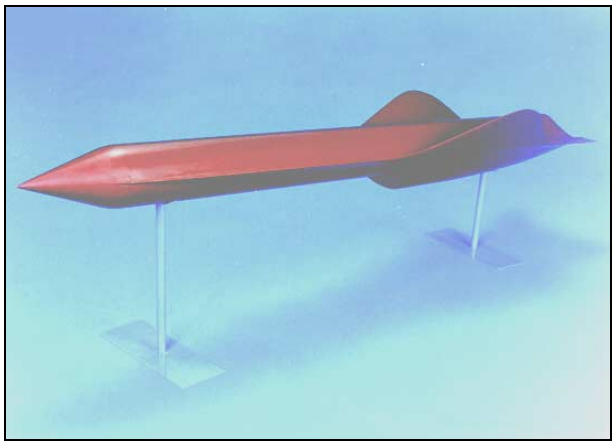

Figure 36 – Stealth Subsonic Cruise missile

Various computations have been run with both the FLU3M and the AEROLOG codes at M = 0.8 and $\beta = 4°$, for different angles of attack. The mesh used is a 4 million point mesh in which the whole boundary layer developments are taken into account (above the fuselage and the fins). The computational time needed to get the results is about 220 hours on one processor of a SGI Origin 2000. Global aerodynamic loads depending on the angle of attack are displayed on figure 37 for the normal force coefficient, on figure 38 for the rolling moment, and on figure 39 for the position of the center of pressure.

The numerical results are in good agreement with the experimental data except for high angles of attack (in absolute value). The average discrepancy on the prediction of the normal force coefficient is about 4%. For the prediction of the position of the center of pressure, the accuracy varies between 0 and 0.4 D. Concerning the prediction of the rolling moment coefficient, the accuracy is about 5%.

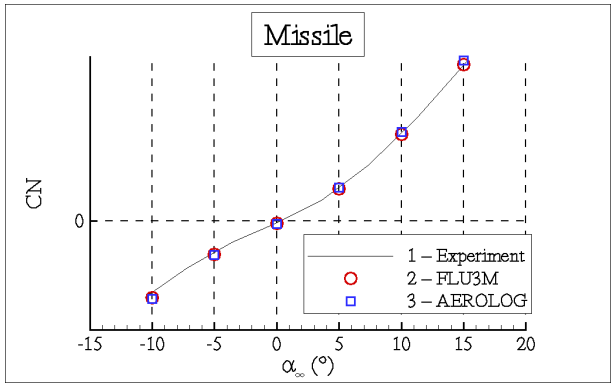

Figure 37 – Stealth Subsonic Cruise missile – Normal force coefficient at M = 0.8, $\beta = 4°$

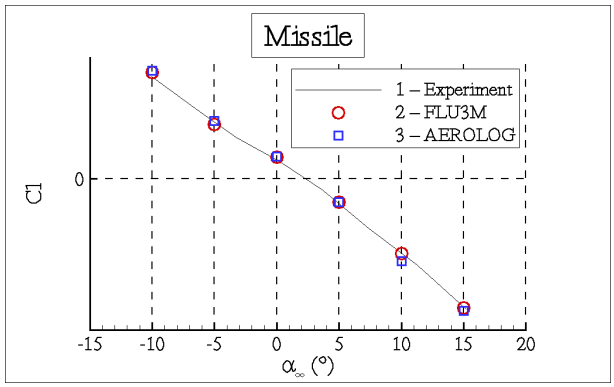

Figure 38 – Stealth Subsonic Cruise missile – Rolling moment coefficient at M = 0.8, $\beta = 4°$

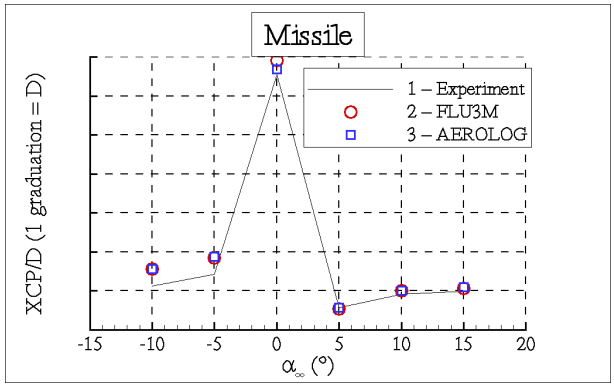

Figure 39 – Stealth Subsonic Cruise missile – Position of the center of pressure at M = 0.8, $\beta = 4°$

On the figures 40 and 41, the total pressure is displayed in two sections of the flow at $\alpha = -10°$. On the first figure, one can distinguish the two forebody vortices and a detached flow on the middle of the fuselage. On the second figure, there is an interaction between the forebody vortices and the fins. The side vortex of the left fin rotates in the same direction as the forebody vortex of this side, whereas both the forebody vortex and side vortex on the right-hand side vanish together.

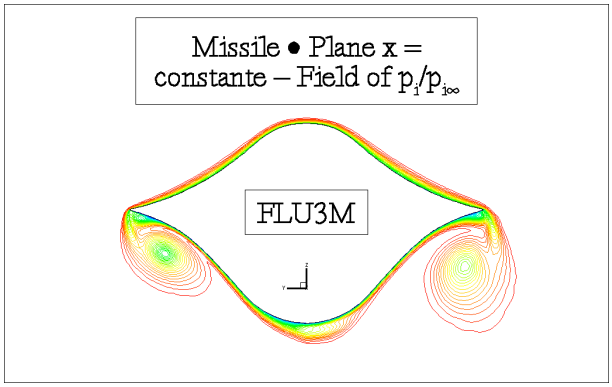

Figure 40 – Stealth Subsonic Cruise missile – Total pressure contours at M = 0.8, $\alpha = -10°$, $\beta = 4°$, X/D = 10

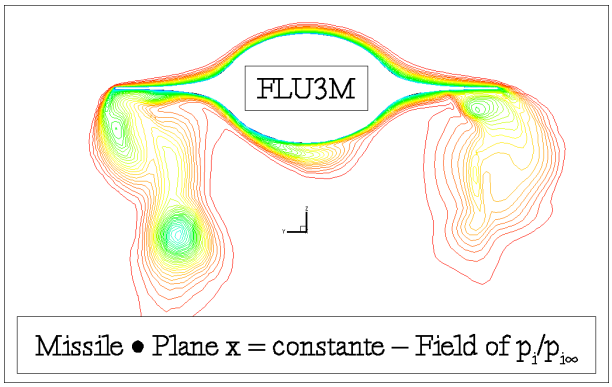

Figure 41 – Stealth Subsonic Cruise missile – Total pressure contours at M = 0.8, $\alpha = -10°$, $\beta = 4°$, X/D = 15

6. CONCLUDING REMARKS

The meshing tool AMCOLI used to refine Euler grids inside the boundary layer regions is operational and has already been successfully used for industrial applications. It allows saving the engineer time spent to generate the Navier-Stokes meshes. The boundary layer flow initialization has not yet been used on industrial configurations even if it has shown some CPU time saving on generic configurations.

The meshing tool AMSITO used to refine Navier-Stokes meshes inside wakes and vortices regions has been used on generic configurations. It still needs to be used on industrial configurations.

The Baldwin-Lomax turbulence model has given accurate results. The prediction of the rolling moment coefficient is much more accurate than before. This may also be due to the fact that computations are now run on much finer meshes. The axial force coefficient prediction still needs to be improved.

The Spalart-Allmaras model which has been developed and validated on generic configurations still needs to be used on industrial ones. It could be used for more complicated problems such as the prediction of the maximal lift of a fin before stall, the computation of fins with gaps, …

A few years ago, Navier-Stokes computations were rarely run for external aerodynamics simulations. This is no longer true. Both industrial companies (EADS Aerospatiale Matra Missiles and MATRA BAe Dynamics France) now use it on a regular basis, thanks to progress made in mesh generation and turbulence modeling, and because they have increased the confidence in the results.

7. ACKNOWLEDGEMENTS

The SIAM contract (n°98.70.505) has been funded by the DGA (SPMT) through collaborations between EADS Aerospatiale Matra Missiles, MATRA BAe Dynamics France and ONERA.

8. REFERENCES

[1] Ben Khelil S., Guillen P., Lazareff M., Lacau R.-G., Numerical Simulation of Roll Induced Moment of Cruciform Tactical Missiles, Aerospace Sciences Technology n°5, 2001

[2] D'Espiney P., Champigny P., Baudin D., Pilon J. A., Couche limite autour d'un fuselage en incidence en écoulement supersonique, RTO Symposium on Missile Aerodynamics, 1998

[3] Brédif M., Chapin F., Borel C., Simon P., Industrial Use of CFD for Missile Studies : New Trends at Matra BAe Dynamics France, RTO Symposium on Missile Aerodynamics, 1998

[4] Deck S., Duveau P., d'Espiney P., Guillen P. Development of Spalart-Allmaras Turbulence Model in FLU3M Code : Towards the Simulation of Complex Aerodynamic Configurations, Submitted to AST

Paper: 15
Author: Mr. Broussard

Question by Mr. Sacher: The prediction of axial force shows the biggest discrepancy. Is this attributed to the missing base flow/drag prediction?

Answer: No, since the base drag is not taken into account concerning the CFD results, the base drag is not computed and not considered in our axial force coefficient. Concerning the experimental data, a correction to the axial force coefficient is added to remove the base drag from the drag coefficient.

This page has been deliberately left blank

Page intentionnellement blanche